ADVANCED THERAPEUTICS
www.advtherap.com

A Nanoparticle Platform for Accelerated In Vivo Oral Delivery Screening of Nucleic Acids

*Rakan El-Mayta, Rui Zhang, Sarah J. Shepherd, Feng Wang, Margaret M. Billingsley, Vadim Dudkin, Donna Klein, Hoang D. Lu, and Michael J. Mitchell**

Oral administration of nucleic acids, such as small interfering RNAs and antisense oligonucleotides, represents a potent modality for treating many gastrointestinal (GI) diseases. However, their use is limited due to a lack of carriers that can effectively mediate their delivery through GI barriers, including gastric enzymes and mucus membranes. Lipid nanoparticles (LNPs) are an emerging delivery system that can protect nucleic acids from degradation and mediate their intracellular delivery, but few studies have evaluated their ability to overcome oral delivery barriers. Here, a high-throughput in vivo screening platform is developed to accelerate the design of LNPs for oral delivery of nucleic acids. A library of LNPs that encapsulate DNA barcodes (b-DNAs) was pooled and orally administered to mice, and their delivery was quantified by deep sequencing. Sequencing results indicated that increases in the molar ratio of cholesterol to lipid-anchored polyethylene glycol conjugate in LNPs enhanced their GI content retention and that the presence of an LNP carrier improved b-DNA delivery to GI tissues, relative to the delivery of naked b-DNA. Collectively, these results suggest that high-throughput in vivo screening can accelerate the discovery of LNPs for GI tract nucleic acid delivery upon oral administration.

1. Introduction

Gastrointestinal (GI) diseases, such as inflammatory bowel disease (IBD), irritable bowel syndrome, and colon cancer, affect millions of people worldwide.[1–5] IBD, for example, is characterized as a chronic inflammatory disease of the GI tract with unknown etiology.[1,2,6] Treatment strategies for IBD include the systemic administration of anti-inflammatory and immunosuppressive drugs, which suppress intestinal inflammatory burden and improve some of the associated symptoms.[7,8] However, these treatments are characterized by limited therapeutic efficacy and adverse systemic effects, such as osteoporosis, hypertension, and increased immunosuppression.[9] These adverse effects are caused, in large part, by off-target drug action and the nonspecificity of treatments. Therefore, the development of novel disease-specific drug delivery strategies is required for more effective and less toxic therapies for treating GI diseases.[7–11]

Nucleic acid therapeutics have emerged as a promising strategy for creating more specific and less toxic therapies as they act specifically in cells expressing their target sequence.[12] Antisense oligonucleotide (ASO) therapy and RNA interference (RNAi) therapy are the two most common approaches for silencing genes that small molecule drugs cannot specifically target.[13–15] The promise of ASO and RNAi therapies for a range of applications has led

R. El-Mayta, Dr. R. Zhang, S. J. Shepherd, M. M. Billingsley, Prof. M. J. Mitchell
Department of Bioengineering
University of Pennsylvania
Philadelphia, PA 19104, USA
E-mail: mjmitch@seas.upenn.edu
Dr. F. Wang
Center for Computational and Genomic Medicine
The Children's Hospital of Philadelphia
Philadelphia, PA 19104, USA
Dr. V. Dudkin, Dr. D. Klein, Dr. H. D. Lu
Janssen Research & Development
Spring House, PA 19477, USA
Prof. M. J. Mitchell
Abramson Cancer Center
Perelman School of Medicine
University of Pennsylvania
Philadelphia, PA 19104, USA
Prof. M. J. Mitchell
Institute for Immunology
Perelman School of Medicine
University of Pennsylvania
Philadelphia, PA 19104, USA
Prof. M. J. Mitchell
Cardiovascular Institute
Perelman School of Medicine
University of Pennsylvania
Philadelphia, PA 19104, USA
Prof. M. J. Mitchell
Institute for Regenerative Medicine
Perelman School of Medicine
University of Pennsylvania
Philadelphia, PA 19104, USA

The ORCID identification number(s) for the author(s) of this article can be found under https://doi.org/10.1002/adtp.202000111

DOI: 10.1002/adtp.202000111

to significant interest in their advancement with many ongoing preclinical studies and clinical trials focused on rare genetic diseases, cancer, and inflammation.[13,16–19] However, these investigations focus mainly on parenteral administration over oral administration—the route of delivery that is considered safer, less expensive, and more convenient for patients.[20,21] Despite the promise of gene therapies, oral delivery of small interfering RNAs (siRNAs) and ASOs remains challenging due to both GI enzyme-mediated nucleic acid degradation and inefficient nucleic acid penetration of the GI mucus for tissue accumulation.[22,23] Therefore, nucleic acids require effective oral drug delivery systems to avoid enzyme-mediated digestion, overcome GI mucus barriers, and facilitate their intracellular delivery into target cells.[24]

Lipid nanoparticles (LNPs) have been widely studied as a nonviral delivery vehicle for nucleic acids, as they can protect their cargo from degradation by nucleases and mediate cytoplasmic delivery.[25–27] Notably, Onpattro (Patisiran), an LNP-based siRNA drug for the treatment of polyneuropathy in patients with hereditary transthyretin-mediated amyloidosis, was approved by the U.S. Food and Drug Administration in 2018—emphasizing the potential for LNP clinical translation.[28] LNPs are commonly formulated with an ionizable lipid component, which aids in LNP endosomal escape and release of nucleic acid cargo into the cytosol. Specifically, these lipids hold a neutral charge under physiological pH,[26] but become positively charged in the acidic endosomal compartment.[29] In addition to the ionizable lipid, LNPs are formulated with an additional three excipients: a cholesterol component to improve LNP stability and enhance membrane fusion;[30] a phospholipid to improve the encapsulation of nucleic acids and promote LNP endosomal escape;[31] and a lipid-anchored polyethylene glycol (PEG) conjugate (lipid-PEG) to minimize LNP aggregation and reduce immune cell opsonization.[32] Slight alterations to any LNP formulation parameters can lead to changes in their physicochemical properties, which can influence their biodistribution and delivery to specific cell types.[33]

To identify LNP candidates for nucleic acid delivery to specific cell types, LNP formulations are typically screened using in vitro assays to identify top candidates that are then further investigated in animal models.[29] In the case of oral delivery, a monolayer of human colon carcinoma cells (Caco-2) is a widely accepted in vitro model for predicting the absorption of orally administered drugs.[34] However, this in vitro model does not fully recapitulate the oral delivery barriers that must be overcome for drugs in vivo. Some of these barriers include: GI-related chemical substances, such as bile salts and pepsin,[22,35] mucus layers, a wide variety of digestive enzymes, and the influence of flow and shear stresses, all of which affect LNP delivery in vivo.[36,37] Therefore, screening LNPs in vitro often fails to accurately predict LNP efficacy in vivo.[38] The development of high-throughput methods for in vivo screening of these delivery systems can facilitate and accelerate the discovery of LNPs that can overcome these delivery barriers and accumulate within GI tissues for gene therapy applications.

Recently, new approaches have been developed for high-throughput screening of NPs in in vivo settings.[39–42] Specifically, molecular barcoding has emerged as a high-throughput method for measuring the biodistribution of libraries of NPs in vivo.[41,43] DNA barcodes (b-DNAs), in combination with polymerase chain reaction (PCR) and deep sequencing, have been specifically utilized for high-throughput LNP screening.[41] Using this approach, LNPs are formulated with unique b-DNAs, after which they can be pooled together and injected as a single dose into mice. Tissues are then isolated from mice and the b-DNAs are recovered, amplified, and sequenced to obtain barcode counts for each sample of interest. Thus, LNPs that interact with target tissues or cells can be identified by their b-DNA via deep sequencing.[44] Through the use of b-DNAs, researchers have gained insight into the underlying mechanisms for how LNP chemistry and structure can affect their in vivo biodistribution.[44]

Here, we utilized this high-throughput approach to screen a library of b-DNA LNPs for GI tract accumulation, as a means to probe for LNP structure–function relationships that confer advantages for oral delivery to GI tissues. Using this approach, we formulated a library of 96 LNP formulations encapsulating b-DNAs, pooled them together, and administered them as a single pool into mice via oral gavage. LNP accumulation in GI tissues was then quantified via deep sequencing, which identified important trends in LNP structural parameters for oral delivery. Specifically, we observed i) increased accumulation of LNPs with high cholesterol content and low lipid-PEG content in the GI content compared to other LNPs, ii) improved b-DNA delivery to GI organs via LNPs by orders of magnitude compared to naked b-DNA, and iii) no correlation between LNP accumulation in a GI organ and LNP accumulation in the contents of that organ, where organ content refers to any material collected as flow through after flushing the organ with phosphate-buffered saline (PBS). These results demonstrate that this platform can be utilized to identify parameters which confer advantages to LNPs for oral delivery, which may be further developed to treat GI-related diseases. This proof-of-concept study suggests that this high-throughput approach can enable and accelerate the screening of LNPs for delivery to GI tissues upon oral administration.

2. Results and Discussion

To probe the structure–function relationships of orally-administered LNPs, we synthesized a library of 96 unique LNP formulations. The LNPs in the library consisted of four components—an ionizable lipid,[45] cholesterol, a helper lipid (1,2-dioleoyl-sn-glycero-3-phosphoethanolamine (DOPE) or 1,2-distearoyl-sn-glycero-3-phosphocholine (DSPC)), and a lipid-PEG (C14-PEG1000, C14-PEG2000, C14-PEG3000, and C14-PEG5000)—combined at six different molar ratios varying only the ratio of cholesterol to lipid-PEG (from 1.5:48.5 to 48.5:1.5). The LNP formulations were mixed at two ionizable lipid:b-DNA weight ratios (5:1 or 10:1) (**Figure 1**A). The 96 LNPs were formulated by pipette mixing and each formulation encapsulated a DNA barcode (b-DNA) (Table S1, Supporting Information). LNPs were characterized for hydrodynamic diameter and polydispersity by dynamic light scattering (DLS), and 94 out of the 96 formulations formed stable LNPs based on DLS analysis of peaks and autocorrelation curves (Table S2, Supporting Information). In general, LNPs formulated with ionizable lipids have a near neutral surface charge at physiological pH.[46–48] In order to significantly change the surface charge of LNPs, research groups have incorporated additional charged excipients, such as 1,2-dioleoyl-3-trimethylammonium-propane

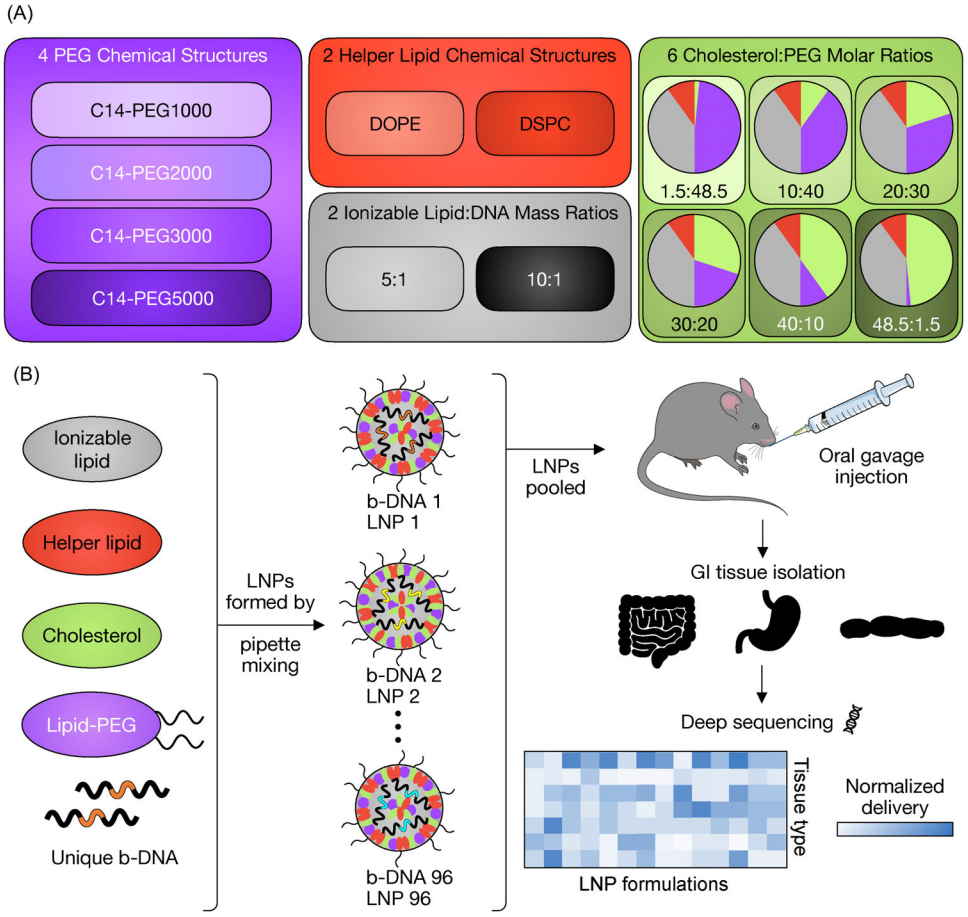

Figure 1. Lipid nanoparticle (LNP) platform for accelerated in vivo oral delivery screening of nucleic acids. A) LNPs were formulated with 4 different lipid-anchored polyethylene glycol (PEG) conjugates (lipid-PEG), 2 different helper lipids, 2 different ionizable lipid:DNA barcode (b-DNA) weight ratio, and 6 different excipient molar ratios varying the ratio of cholesterol to lipid-PEG, for a total of 96 LNP formulations. Details on specific excipient molar ratios for each LNP are provided in Table S1 (Supporting Information). B) LNPs were formulated by pipette mixing to encapsulate barcoded DNA (b-DNA). LNP formulations were pooled together and administered orally to C57BL/6 mice via oral gavage ($N = 4$). Tissues were isolated 6 h postinjection, DNA was extracted, and accumulation of b-DNAs was quantified by deep sequencing.

(DOTAP) and 1,2-dioleoyl-sn-glycero-3-phosphate (18PA), to increase or decrease the surface charge, respectively.[49,50] In this study, we did not examine the effects of surface charge, but future work will investigate the effects of this parameter as it pertains to mucus penetration and tissue accumulation.[51] These 94 LNPs were pooled together, along with naked b-DNA, and administered via oral gavage into mice ($N = 4$) at a dose of 0.4 µg per b-DNA. 6 h post-administration, GI organs (stomach, small intestine, cecum, and colon) and content (flushed from small intestine and colon) were isolated from mice, DNA was extracted, b-DNAs were amplified by PCR, and LNP accumulation was quantified by deep sequencing (Figure 1B). Small intestine content and colon content refers to any material that was collected as flow through from inside the small intestine and colon sections, respectively, of the GI tract.

Since GI transit time in mice is ≈6 h, the majority of orally administered LNPs should be excreted within 6 h.[20,52] Previous research demonstrated that particulate engineering may be beneficial for maximizing delivery to GI tissues.[20,21,53,54] For this reason, LNP accumulation in the stomach, small intestine content, cecum, and colon content was assessed via deep sequencing and data were displayed using a heat map (**Figure 2**A). Because the majority of drug absorption occurs in the small intestine and colon, we adapted an existing protocol to be able to separate these tissues from their content.[55,56] Given that the stomach is mostly a processing organ and both the stomach and cecum are difficult to thoroughly flush with a syringe, we processed these organs whole and only separated the small intestine and colon from their contents by flushing with PBS.[55,57]

Deep sequencing results indicated that LNPs formulated with a higher molar ratio of cholesterol to lipid-PEG accumulated to a greater extent in these tissues relative to LNPs formulated with a lower molar ratio of cholesterol to lipid-PEG. To better assess this structure–function relationship, we grouped LNP formulations based on the molar ratio of cholesterol to lipid-PEG and indicated the PEG molecular weight of each LNP (Figure 2B). Additionally, we identified and listed the top ten LNPs in each category for a more detailed quantitative analysis (**Table 1**A and 1B; and Table S3, Supporting Information). For these samples (the stomach, small intestine content, cecum, and colon content), seven of

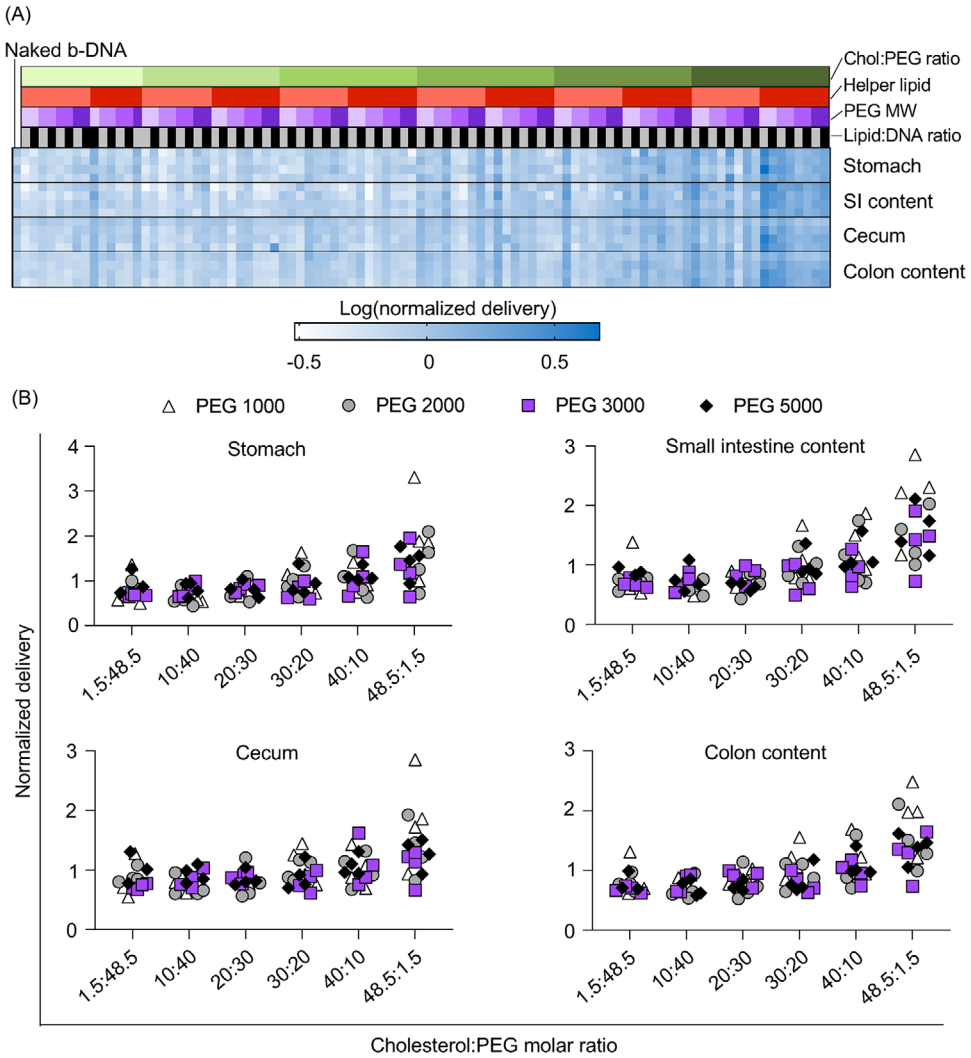

Figure 2. Effects of cholesterol and lipid-PEG composition on LNP accumulation in the stomach, small intestine content, colon content, and cecum. A) Along with naked b-DNA, 94 LNP formulations were pooled together and administered orally via oral gavage to C57BL/6 mice ($N = 4$). Tissues were isolated 6 h post-administration and DNA was extracted for deep sequencing. A heatmap representing accumulation of LNPs to different tissues was generated. Darker clusters represent higher accumulation of a b-DNA in a particular tissue sample. LNP formulations are described above the heatmap. Cholesterol to lipid-PEG molar ratio: light green to dark green represents increases in the molar percentage of cholesterol incorporated into LNPs from 1.5%, 10%, 20%, 30%, 40%, to 48.5%. Helper Lipid: light red = DOPE, dark red = DSPC. PEG molecular weight: Light purple to dark purple represents increasing values from 1000, 2000, 3000, to 5000 Da. Ionizable lipid:b-DNA weight ratio: white = 5:1, black = 10:1. B) LNP delivery to these organs was grouped by their cholesterol to lipid-PEG molar percentage in order to visualize the effects of increasing molar ratios. The PEG molecular weight incorporated into the LNP was also identified. White triangle = PEG 1000 Da, gray circle = PEG 2000 Da, blue square = PEG 3000 Da, and black diamond = PEG 5000 Da. All sequencing data were normalized to the uninjected pool of LNPs.

Table 1A. The top ten LNP formulations for accumulation to the stomach, small intestine content, cecum, and colon content were identified and categorized by different cholesterol:lipid-PEG molar ratios. Specific formulations are described further in Tables S1 and S3 (Supporting Information).

	1.5% Cholesterol/ 48.5% lipid-PEG	10% Cholesterol/ 40% lipid-PEG	20% Cholesterol/ 30% lipid-PEG	30% Cholesterol/ 20% lipid-PEG	40% Cholesterol/ 10% lipid-PEG	48.5% Cholesterol/ 1.5% lipid-PEG
Stomach	0	0	0	1	2	7
Small intestine content	0	0	0	1	2	7
Cecum	0	0	0	1	2	7
Colon content	0	0	0	1	2	7

Table 1B. The top ten LNP formulations for accumulation to the stomach, small intestine content, cecum, and colon content were identified and categorized by different PEG molecular weights. Specific formulations are described further in Tables S1 and S3 (Supporting Information).

	PEG1000	PEG2000	PEG3000	PEG5000
Stomach	4	3	2	1
Small intestine content	5	2	1	2
Cecum	5	2	1	1
Colon content	5	3	1	1

the ten lead LNPs were formulated with 48.5% cholesterol and 1.5% lipid-PEG. Additionally, none of the top ten lead formulations contained less than 30% cholesterol or more than 20% lipid-PEG (Table 1A). Taken together, these results suggest that LNPs with high cholesterol content and low lipid-PEG content accumulated more in these tissue samples compared to other LNP formulations. Higher cholesterol content may improve the hydrophobicity of LNPs, and improve both stability and accumulation, consistent with previous observations.[58–62] Nearly half of the top ten lead formulations contained the shortest PEG chain utilized in this study—PEG1000 (Table 1B). Shorter PEG MW at high density can result in improved mucus penetration and accumulation in the GI tract tissue,[63] but at low density penetration is hindered which results in content accumulation. Additionally, we examined the top ten formulations further to determine if there existed differences in the identity of the helper lipid. Of the top ten lead LNPs to each tissue sample, approximately seven out of the ten were formulated with the helper lipid DSPC (Table S4, Supporting Information).

Following deep sequencing, we compared LNP accumulation in both the stomach and cecum using an unpaired *t*-test. We identified one LNP formulation that accumulated the most in both organs relative to the other LNPs (LNP 71) and one LNP with low accumulation in both organs (LNP 26) (**Figure 3**A). In order to validate the deep sequencing data for these two LNPs, we performed another in vivo experiment where we orally administered each LNP to a single group of mice. The whole stomach and whole cecum were isolated as before with their respective contents 6 h post-administration, and total b-DNAs present were amplified by quantitative polymerase chain reaction (qPCR) (Figure 3B). LNP 71 accumulated more than LNP 26 in both the stomach (****$P < 0.0001$) and cecum ($P = 0.069$) (Figure 3C,D).

Next, we examined LNP accumulation in the small intestine and colon. These tissue samples were examined separately due to being flushed thoroughly of any content. Within the heat map, darker blue indicated higher accumulation to a tissue of interest. The darker blue clusters were dispersed across LNPs, indicating few consistent trends in structure–function relationships (**Figure 4**A). Similar to our previous method of analysis, we grouped LNPs based on the molar ratio of cholesterol to lipid-PEG and identified the molecular weight of the PEG chain used in each LNP (Figure 4B). Unlike the deep sequencing analysis of the content/content-containing tissues, the small intestine and colon contain no trends with respect to changes in the molar ratio of cholesterol to lipid-PEG. Mucus membranes are known for having the ability to capture and remove foreign molecules and hydrophobic particles,[60] but previous research has demonstrated that PEGylation of NPs allows for carriers to navigate mucus membranes and reach the underlying epithelium.[20,60,64] Although this is a preliminary study investigating the use of ionizable LNPs for oral delivery, several research groups have examined how PEG density and molecular weight impacts mucoadhesion of nanoparticulates and allows for penetration through mucus to target tissues.[65,66] One research report found that nanoparticles that were partially coated with a low molecular weight PEG significantly decreased the average transport rate compared to nanoparticles that were fully coated with the low molecular weight PEG.[60] Additionally, increasing the PEG molecular weight resulted in a significant reduction in transport.[60] Both of these results suggest that low molecular weight PEG and a high surface density of PEG is required for rapid penetration of mucus.[60] For LNPs, it is therefore possible that there exists a balance between hydrophobic (interior components improving stability) and hydrophilic components (surface components improving mucus penetration) that allows them to accumulate in the underlying tissue.[67,68] This provides insight into why there are no visible trends in the heatmap for the small intestine and colon; as the molar ratio of cholesterol to lipid-PEG is increased, LNPs contain more interior components that improve stability, but contain less surface components to improve mucus penetration. Conversely, as the molar ratio of cholesterol to lipid-PEG is decreased, LNPs contain fewer interior components to improve stability and more surface components to improve mucus penetration. Future work aims to examine how this balance influences the penetration of LNPs into the epithelium of these tissues. For a more quantitative analysis, we identified and listed the top ten LNPs that accumulated in the small intestine and colon (**Table 2**A and 2B; and Table S3, Supporting Information). In both organs, six out of the top ten LNPs had a cholesterol content of 30% or more (Table 2A). Furthermore, eight out of ten LNPs and nine out of ten LNPs were formulated with a PEG length of 2000 Da or less in the small intestine and colon, respectively (Table 2B). Additionally, we examined the top ten formulations further to determine if there existed differences in the identity of the helper lipid. Of the top ten lead LNPs to each tissue sample, there was practically an even split of LNPs formulated with DOPE and LNPs formulated with DSPC (Table S4, Supporting Information).

Following deep sequencing, we quantified and plotted accumulation of LNPs in the small intestine and colon. We identified a lead formulation, LNP 67, that was highly enriched in both tissues (**Figure 5**A). Since this LNP was the top performer in both tissues, we sought to examine how well it accumulated compared to the naked b-DNA, the negative control in this experiment. Individually comparing the deep sequencing data of the b-DNA-encapsulating LNP to the naked b-DNA using an unpaired *t*-test, we can quantitatively measure a fold increase in performance due to the presence of the LNP. In the small intestine, LNP 67 accumulated ≈101 times more than the naked b-DNA (****$P < 0.0001$) (Figure 5B), while the LNP saw a 33-fold increase over naked b-DNA in the colon (***$P < 0.001$) (Figure 5C). Collectively, these data suggest that the use of an LNP carrier can greatly improve accumulation.

Finally, we sought to explore if any correlations existed in LNP accumulation between GI tissues and their content. We plotted

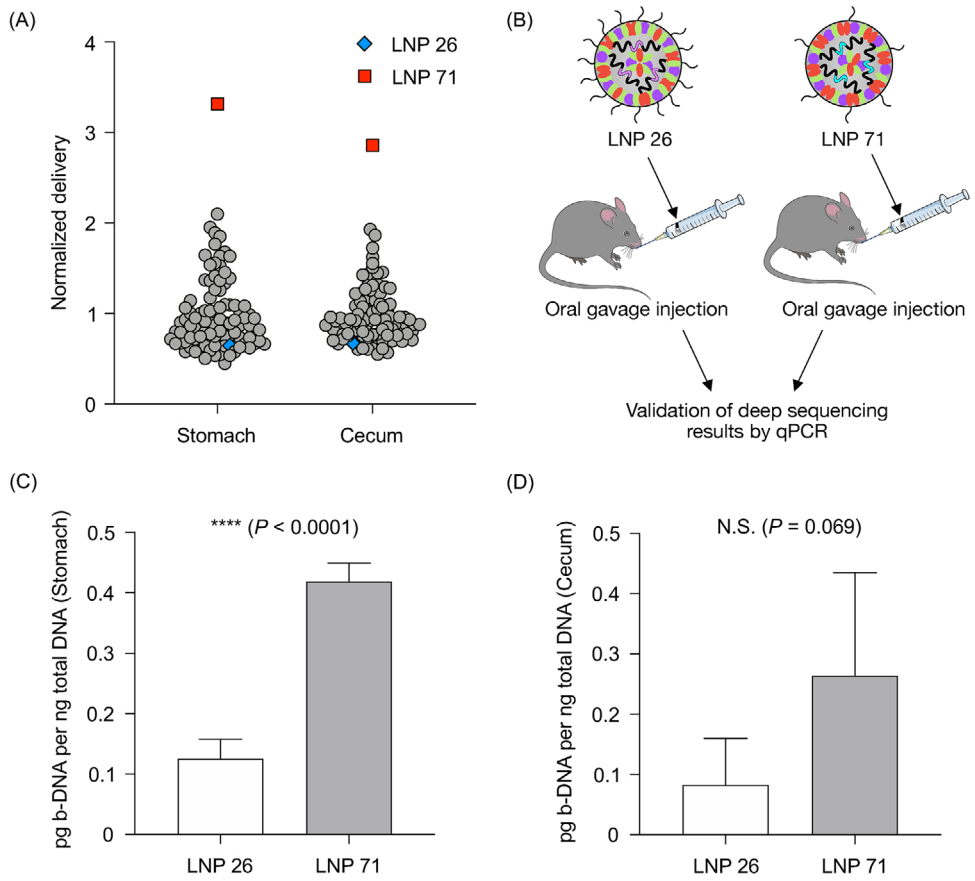

Figure 3. Quantitative polymerase chain reaction (qPCR) results validate deep sequencing results of high-throughput in vivo screening. A) Along with a naked b-DNA, 94 LNP formulations were pooled together and administered orally via oral gavage to C57BL/6 mice ($N = 4$). Tissues were isolated 6 h post-administration and DNA was extracted for deep sequencing. Accumulation of b-DNAs in the stomach and cecum was plotted. B) In order to validate sequencing results using qPCR, specific LNPs were orally administered to different groups of C57BL/6 mice ($N = 4$). Tissues were isolated, DNA was extracted, and 5 ng of extracted DNA was used to amplify and quantify total b-DNAs present. C) In the stomach, LNP 71 accumulated more than LNP 26 (****$P < 0.0001$). D) In the cecum, LNP 71 accumulated more than LNP 26 ($P = 0.069$). Data were plotted as mean ± SD. N.S. denotes not significant, and ****$P < 0.0001$ by unpaired t-test.

Table 2A. The top ten LNP formulations for accumulation to the small intestine and colon were identified and categorized by different cholesterol:lipid-PEG molar ratios. Specific formulations are described further in Tables S1 and S3 (Supporting Information).

	1.5% Cholesterol/ 48.5% lipid-PEG	10% Cholesterol/ 40% lipid-PEG	20% Cholesterol/ 30% lipid-PEG	30% Cholesterol/ 20% lipid-PEG	40% Cholesterol/ 10% lipid-PEG	48.5% Cholesterol/ 1.5% lipid-PEG
Small Intestine	2	2	0	2	2	2
Colon	2	2	0	1	3	2

Table 2B. The top ten LNP formulations for accumulation to the small intestine and colon were identified and categorized by different PEG molecular weights. Specific formulations are described further in Tables S1 and S3 (Supporting Information).

	PEG1000	PEG2000	PEG3000	PEG5000
Small Intestine	5	3	2	0
Colon	6	3	1	0

normalized delivery to colon content against normalized delivery to small intestine content and found that LNP accumulation positively correlated ($R^2 = 0.900$), indicating that LNPs collected in the content of the small intestine were likely unable to penetrate the mucus membrane and reach the underlying tissue (**Figure 6**A). We then plotted normalized delivery to the colon against normalized delivery to the small intestine and found a strong positive correlation for LNP accumulation in both tissues ($R^2 = 0.952$), indicating that LNPs that were able to traverse the

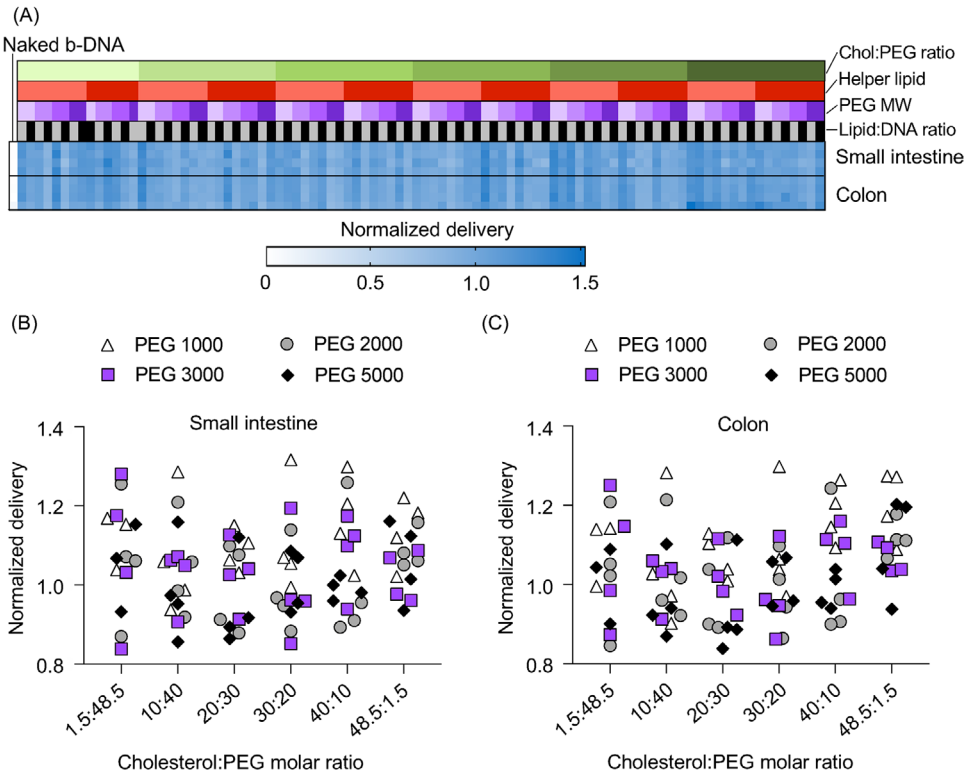

Figure 4. Effects of cholesterol and lipid-PEG composition on LNP accumulation in the small intestine and colon. A) Along with a naked b-DNA, 94 LNP formulations were pooled together and administered orally via oral gavage to C57BL/6 mice ($N = 4$). Tissues were isolated and flushed 6 h post-administration, and DNA was extracted for deep sequencing. A heatmap representing accumulation of LNPs to different tissues was generated. Darker clusters represent higher accumulation of a b-DNA in a particular tissue sample. LNP formulations are described above the heatmap. Cholesterol to lipid-PEG molar ratio: light green to dark green represents increases in the molar percentage of cholesterol incorporated into LNPs from 1.5%, 10%, 20%, 30%, 40%, to 48.5%. Helper Lipid: light red = DOPE, dark red = DSPC. PEG molecular weight: Light purple to dark purple represents increasing values from 1000, 2000, 3000, to 5000 Da. Ionizable lipid:b-DNA weight ratio: white = 5:1, black = 10:1. B,C) LNP delivery to these organs was grouped by their cholesterol to lipid-PEG molar percentage in order to visualize the effects of increasing molar ratios. The PEG molecular weight incorporated into the LNP was also identified. White triangle = PEG 1000 Da, gray circle = PEG 2000 Da, blue square = PEG 3000 Da, and black diamond = PEG 5000 Da. All sequencing data were normalized to the uninjected pool of LNPs.

mucus and reach target tissues were able to accomplish this throughout both tissues (Figure 6B). However, when examining the relationship between delivery to the small intestine and its content and the colon and its content, we find no correlation in accumulation between the two ($R^2 = 0.012$ and $R^2 = 0.037$, respectively) (Figure 6C,D). This relationship is complex and influenced by a variety of factors in vivo. As such, high accumulation in tissue content could refer to low tissue penetration or high mucus trapping, while low accumulation in the content could indicate high tissue penetration or higher excretion rates through the feces. This points to different design spaces for accomplishing tissue-specific accumulation versus accumulation in luminal contents. Stability can improve cargo accumulation in luminal contents, while both stability and mucus penetration can improve cargo accumulation to tissues itself.[58–62]

3. Conclusion

Here, we demonstrated that molecular barcoding can enable high-throughput screening of a library of LNPs following oral administration. This platform enabled us to develop structure–function relationships between the physicochemical properties of LNPs and their biodistribution in the GI tract. Specifically, increasing the molar ratio of cholesterol to lipid-PEG in LNPs increased their retention in the GI tract as demonstrated by their presence in GI content 6 h post-administration. For accumulation in the small intestine and colon tissues, the ratio of hydrophobic to hydrophilic components (cholesterol to lipid-PEG) in LNPs seemed to be less predictive in assessing LNP accumulation, but a balance of hydrophobic and hydrophilic components may confer both stability and mucus-penetration abilities to LNPs so that they may be retained longer in the GI tract and accumulate in these tissues more effectively.[60,65] Future works aims to further investigate this balance as it relates to oral delivery of nanoparticulate-based delivery systems. This proof-of-concept study demonstrates that high-throughput in vivo screening can be used to identify favorable LNP characteristics for oral administration of nucleic acids and parameters in nanoparticle design that may be important for delivery to GI tissues.

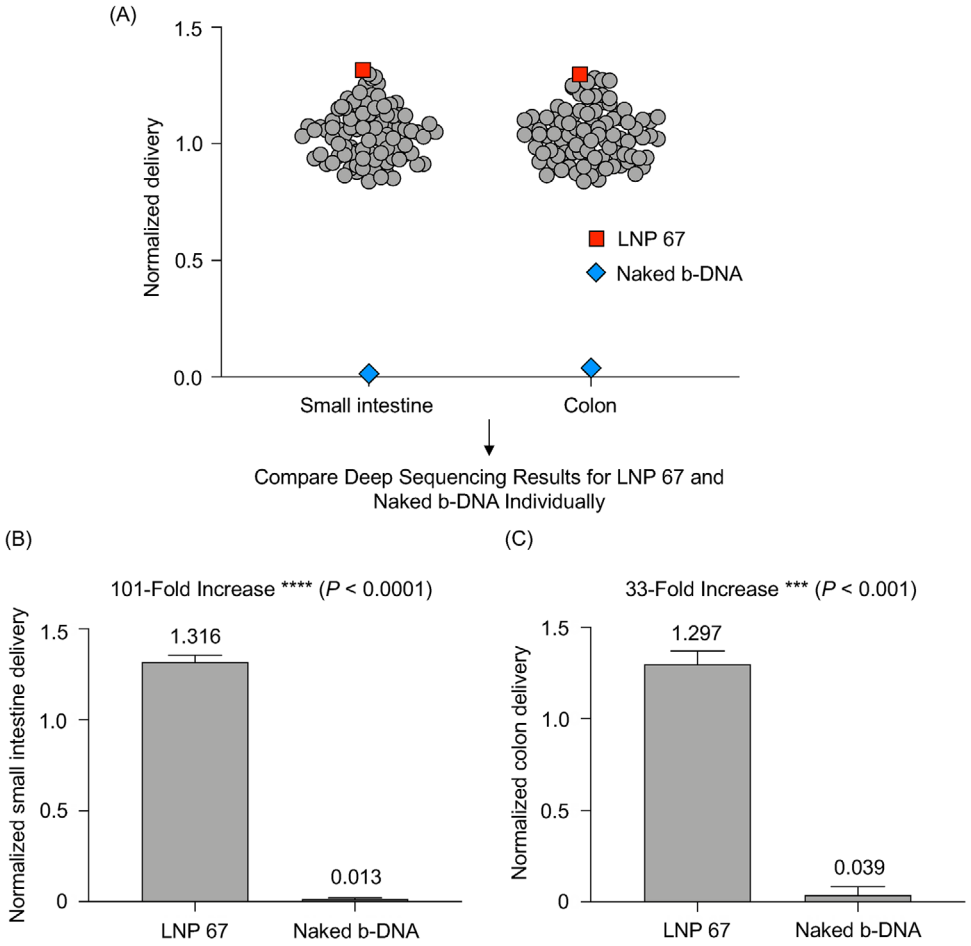

Figure 5. Comparison of LNP and naked b-DNA accumulation in the small intestine and colon following high-throughput in vivo screening. A) Along with a naked b-DNA, 94 LNP formulations were pooled together and administered orally via oral gavage to C57BL/6 mice ($N = 4$). Tissues were isolated 6 h post-administration and DNA was extracted for deep sequencing. Accumulation of b-DNAs in the small intestine and colon was plotted and a lead LNP was identified. B,C) The lead LNP formulation for delivery to these organs (LNP 67) was compared to the naked b-DNA directly. LNP 67 improved delivery to the B) small intestine and C) colon by 101-fold (****$P < 0.0001$) and 33-fold (***$P < 0.001$), respectively. Data were plotted as mean ± SD. ***$P < 0.001$ and ****$P < 0.0001$ by unpaired t-test.

4. Experimental Section

DNA Barcode (b-DNA) Design: b-DNAs were single-stranded DNAs that consisted of 61 nucleotides with five consecutive phosphorothioate bonds at each end.[43] The barcode region was composed of 10 nucleotides in the center of the oligonucleotide. An additional 10 random nucleotides were included at 3′ end of the barcode region. The 5′ and 3′ ends of each b-DNA were conserved and contained priming sites for Illumina adapters. A full list of b-DNA sequences can be found in Table S5 (Supporting Information). All oligonucleotides in this study were synthesized and purified (standard desalting procedure) by Integrated DNA Technologies.

Ionizable Lipid Synthesis and Characterization: Briefly, epoxide-terminated alkyl chains (Sigma-Aldrich) were reacted with polyamine cores by Michael addition chemistry. The reagents were reacted at a 7-molar excess of alkyl chains at 80 °C for 48 h. The resulting lipids were mixed with Celite 545 (Sigma-Aldrich) and all solvent was evaporated using a Rotavapor R-300 (BÜCHI). The ionizable lipid was purified by using a CombiFlash Nextgen 300+ chromatography system (Teledyne ISCO) and target fractions were identified by liquid chromatography-mass spectrometry.

LNP Formulation and Characterization: The lipid solution was made by dissolving ionizable lipid, helper lipid, cholesterol, and PEG-lipid in ethanol at given molar ratios shown in Table S1 (Supporting Information). b-DNAs were dissolved in citrate buffer (10×10^{-3} M, pH 4.0) at weight ratios of 5:1 or 10:1 (ionizable lipid:b-DNA). LNPs were formulated by pipette mixing the lipid solution into the nucleic acid-containing citrate buffer at a volume ratio of 3:1 (citrate buffer:ethanol, v/v). The resulting LNPs were dialyzed against PBS in a 96-well microdialysis plate (10 000 MWCO, Thermo Fisher Scientific, 88 260) at room temperature for 2 h. Cholesterol was purchased from Sigma-Aldrich (C8667). Other lipid components, including helper lipid and PEG-lipid, were obtained from Avanti Polar Lipids: 1,2-dioleoyl-sn-glycero-3-phosphoethanolamine (850725P), 1,2-distearoyl-sn-glycero-3-phosphocholine (850365P), 1,2-dimyristoyl-sn-glycero-3-phosphoethanolamine-N-[methoxy(polyethylene glycol)-1000] (ammonium salt) (C14-PEG1000, 880710P), 1,2-dimyristoyl-sn-glycero-3-phosphoethanolamine-N-[methoxy(polyethylene glycol)-2000] (ammonium salt) (C14-PEG2000, 880150P), 1,2-dimyristoyl-sn-glycero-3-phosphoethanolamine-N-[methoxy(polyethylene glycol)-3000] (ammonium salt) (C14-PEG3000, 880310P), and 1,2-dimyristoyl-sn-glycero-3-phosphoethanolamine-N-[methoxy(polyethylene glycol)-5000] (ammonium salt) (C14-PEG5000, 880210P). DNA concentration in LNP

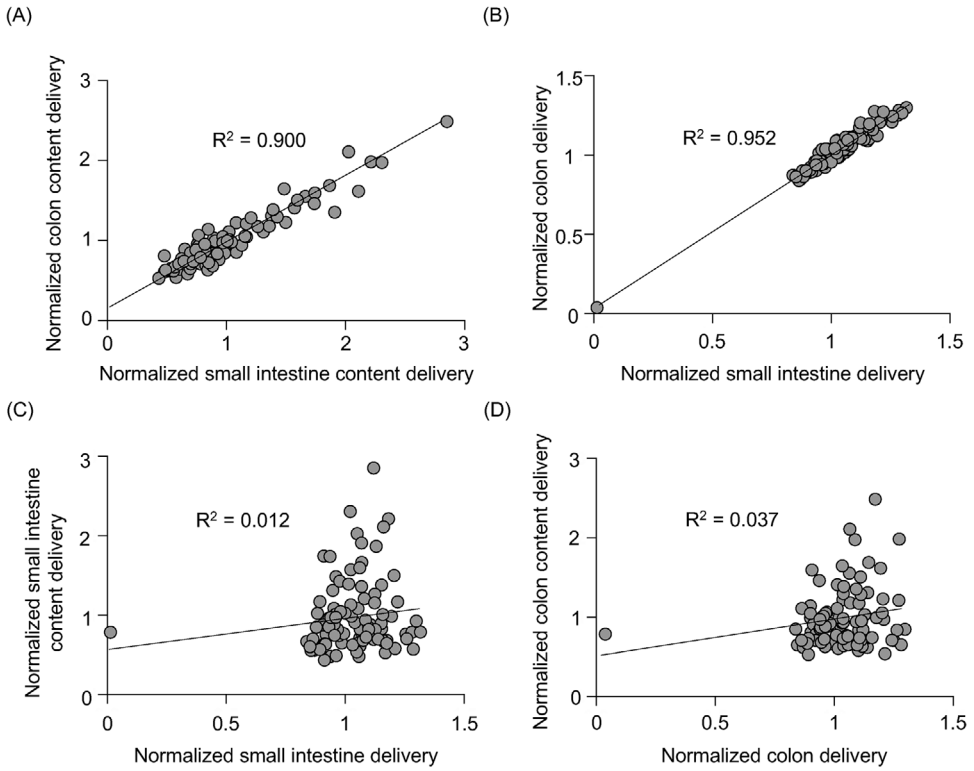

Figure 6. Correlations between LNP delivery to the small intestine, colon, and their contents. A–D) Along with a naked b-DNA, 94 LNP formulations were pooled together and administered orally via oral gavage to C57BL/6 mice ($N = 4$). Tissues were isolated 6 h post-administration and DNA was extracted for deep sequencing. Accumulation of b-DNAs between various tissues was plotted. Each data point represents the average normalized delivery of a particular LNP across the four mice. A) Normalized delivery to the colon content was plotted against normalized delivery to the small intestine content ($R^2 = 0.900$). B) Normalized delivery to the colon was plotted against normalized delivery to the small intestine ($R^2 = 0.952$). C) Normalized delivery to the small intestine content was plotted against normalized delivery to the small intestine ($R^2 = 0.012$). D) Normalized delivery to the colon content was plotted against normalized delivery to the colon ($R^2 = 0.037$). R^2 values were calculated following a linear regression model.

formulations was determined using a NanoDrop Spectrophotometer (Thermo Fisher Scientific). LNP hydrodynamic diameter and polydispersity were measured using a Zetasizer Nano ZS instrument (Malvern Panalytical).

Animal Experiments: All procedures were performed under an animal protocol approved by the University of Pennsylvania Institutional Animal Care and Use Committee (IACUC). To evaluate LNP biodistribution using deep sequencing, 8-week-old female C57BL/6 mice (Jackson Laboratory, 18–21 g) were orally administered with a pool of different b-DNA LNPs, along with a naked b-DNA (served as a negative control), at the amount of 0.4 µg per each b-DNA. To validate deep sequencing results using qPCR, mice were orally administered with either a single b-DNA LNP formulation or a naked b-DNA, at the amount of 20 µg b-DNA per injection. For all experiments, tissue samples were harvested 6 h post-administration, snap-frozen in liquid nitrogen, disrupted into powder using a Geno/Grinder (SPEX Sample Prep), and stored in a −80 °C freezer until further analyzed.

b-DNA Library Preparation: To extract DNA from a tissue sample, ≈30 mg of disrupted frozen tissue was resuspended in lysis buffer that contained 100×10^{-3} M Tris-HCl (Fisher Scientific, 50 155 887), 5×10^{-3} M ethylenediaminetetraacetic acid (EDTA) (Fisher Scientific, 50 997 738), 0.2% sodium dodecyl sulfate (SDS) (Fisher Scientific, 507 513 793), 200×10^{-3} M NaCl (Fisher Scientific, S318100), and 0.2 mg mL^{-1} proteinase K (Thermo Fisher Scientific, PI17916).[69] Extracted DNA was further purified by Zymo Oligo Clean and Concentrator columns (Zymo Research, D4060) according to the manufacturer's instructions. b-DNA amplification was conducted by PCR using the following reagents: 5 µL 5X HF Phusion buffer, 0.5 µL 10×10^{-3} M dNTPs, 0.25 µL Phusion High-Fidelity DNA Polymerase (Thermo Fisher Scientific, F530S), 1.18 µL extracted DNA, 1 µL 5×10^{-6} M forward primer, 1 µL 5×10^{-6} M reverse primer, 2 µL dimethylsulfoxide (DMSO), and 15.25 µL H_2O. PCR cycling conditions were 98 °C for 12 s, 67 °C for 22 s, and 72 °C for 28 s, for a total of 35 cycles. Primer sequences are shown below:

Forward Primer: 5'-AATGATACGGCGACCACCGAGATCTACACTCTTTCCCTACACGACGCTCTTCCGATCT.

Reverse Primer: 5'-CAAGCAGAAGACGGCATACGAGATXXXXXXXXGTGACTGGAGTTCAGACGTGTGCTCTTCCGATCT.

XXXXXXXX: denotes an 8 nucleotide organ barcode. The full list of full-length reverse primers can be found in Table S6 (Supporting Information).

PCR products were run by gel electrophoresis on 3% agarose (Universal Medical, IB70060) in Tris-acetate-EDTA buffer (Fisher Scientific, 24 710 030). Amplified b-DNA (144bp) was excised from the gel, pooled, and purified by Zymo Gel Extraction columns (Zymo Research, D4001) according to the manufacturer's protocol. The purified products were kept frozen at −20 °C until deep sequencing.

Deep Sequencing and Barcode Delivery Quantification: All deep-sequencing runs were performed using multiplexed runs on Illumina MiSeq (Illumina). PCR product pools were quantitated using the KAPA Library Quantification Kit for next-generation sequencing. PCR product pools were loaded onto flow cells at 4×10^{-3} M concentration.

b-DNA delivery of a specific barcode to a certain tissue was calculated according to the following 3 steps: i) dividing the number of sequencing reads of one barcode delivered by a single LNP formulation by the total amount of reads from all barcodes delivered by all LNPs in a specific tissue; ii) dividing the number of sequencing reads of the same barcode (utilized

in (i)) by the total amount of reads from all barcodes of all LNPs in the noninjected LNP pool . iii) Dividing the results from (i) by the results from (ii).

qPCR: Primer sequences were designed using Primer-BLAST (National Institute of Health). Both forward primer and reverse primer sequences were designed to bind the conserved region of b-DNA. Primer sequences are shown below:

Forward Primer: 5'-AGACGTGTGCTCTTCCGAT.

Reverse Primer: 5'-ACACGACGCTCTTCCGAT.

qPCR was performed using Fast SYBR Green Master Mix (Thermo Fisher Scientific, 4 385 612). qPCR master solution was prepared as follows: 10 µL Fast SYBR Green Master Mix (2X), 1 µL 5×10^{-6} M forward primer, 1 µL 5×10^{-6} M reverse primer, 3 µL molecular biology grade water. Subsequently, 5 µL of 1 ng μL^{-1} extracted DNA from each tissue sample were mixed with 15 µL qPCR master solution, reaching a final volume of 20 µL. To make the qPCR reaction solution for a calibration curve, 5 µL b-DNA of known concentrations were made by serial dilution and mixed with 15 µL of the same qPCR master solution. The cycling conditions were carried out following the manufacturer's protocol: after 20 s of denaturation at 95 °C, 50 cycles with 2-segment amplification were performed consisting of 3 s at 95 °C for denaturation and 30 s at 60 °C for polymerase elongation.

After the qPCR reaction, a calibration curve was generated by plotting the logarithm of the concentrations of b-DNA standard and their corresponding value of cycle threshold (Ct). This calibration curve was then used to determine the b-DNA concentration of tissue samples. For all the tissue samples, a total of 5 ng of extracted DNA was added for each reaction. Therefore, the amount of b-DNA in each tissue sample was normalized to picogram b-DNA per ng total extracted DNA.

Statistical Analysis: Statistical tests were performed in Graphpad Prism 8. Data were plotted as mean ± SD. Each group contained an $N = 4$. Differences between groups were determined using an unpaired *t*-test. $*P < 0.05$, $**P < 0.01$, $***P < 0.001$, $****P < 0.0001$, and N.S. denoted not significant.

Supporting Information

Supporting Information is available from the Wiley Online Library or from the author.

Acknowledgements

R.E. and R.Z. contributed equally to this work. This study was supported by Janssen Research and Development. Thanks to Jason Riggs, Michele Rizzolio, Avijit Ghosh, Mihee Kim, and William Kintigh for insight and assistance on this manuscript.

Conflict of Interest

The authors declare no conflict of interest.

Keywords

DNA barcoding, drug delivery, high-throughput screening, lipid nanoparticles, oral delivery

Received: May 15, 2020
Revised: July 28, 2020
Published online: August 31, 2020

[1] L. Ricci-Vitiani, D. G. Lombardi, E. Pilozzi, M. Biffoni, M. Todaro, C. Peschle, R. De Maria, *Nature* **2007**, *445*, 111.
[2] B. Khor, A. Gardet, R. J. Xavier, *Nature* **2011**, *474*, 307.
[3] R. J. Xavier, D. K. Podolsky, *Nature* **2007**, *448*, 427.
[4] F. Klem, A. Wadhwa, L. J. Prokop, W. J. Sundt, G. Farrugia, M. Camilleri, S. Singh, M. Grover, *Gastroenterology* **2017**, *152*, 1042.
[5] M. Avramidou, F. Angst, J. Angst, A. Aeschlimann, W. Rössler, U. Schnyder, *BMC Gastroenterol.* **2018**, *18*, 21.
[6] D. C. Baumgart, S. R. Carding, *Lancet* **2007**, *369*, 1627.
[7] J. Cosnes, C. Gowerrousseau, P. Seksik, A. Cortot, *Gastroenterology* **2011**, *140*, 1785.
[8] J. K. Triantafillidis, E. Merikas, F. Georgopoulos, *Drug Des., Dev. Ther.* **2011**, *5*, 185.
[9] P. A. Dugué, M. Rebolj, P. Garred, E. Lynge, *Expert Rev. Anticancer Ther.* **2013**, *13*, 29.
[10] G. Pasternak, D. Aebisher, R. Filip, D. Bartusik-Aebisher, *Eur. J. Clin. Exp. Med.* **2019**, *16*, 341.
[11] O. S. Fenton, K. N. Olafson, P. S. Pillai, M. J. Mitchell, R. Langer, *Adv. Mater.* **2018**, *30*, 1705328.
[12] R. M. Haley, R. Gottardi, R. Langer, M. J. Mitchell, *Drug Delivery Transl. Res.* **2020**, *10*, 661.
[13] X. Shen, D. R. Corey, *Nucleic Acids Res.* **2018**, *46*, 1584.
[14] R. Kanasty, J. R. Dorkin, A. Vegas, D. Anderson, *Nat. Mater.* **2013**, *12*, 967.
[15] K. A. Whitehead, R. Langer, D. G. Anderson, *Nat. Rev. Drug Discovery* **2009**, *8*, 129.
[16] A. de Fougerolles, H. P. Vornlocher, J. Maraganore, J. Lieberman, *Nat. Rev. Drug Discovery* **2007**, *6*, 443.
[17] A. Aartsma-Rus, *Nucleic Acid Ther.* **2017**, *27*, 67.
[18] R. Kole, A. R. Krainer, S. Altman, *Nat. Rev. Drug Discovery* **2012**, *11*, 125.
[19] R. S. Riley, C. H. June, R. Langer, M. J. Mitchell, *Nat. Rev. Drug Discovery* **2019**, *18*, 175.
[20] K. Maisel, L. Ensign, M. Reddy, R. Cone, J. Hanes, *J. Controlled Release* **2016**, *197*, 48.
[21] L. M. Ensign, R. Cone, J. Hanes, *Adv. Drug Delivery Rev.* **2012**, *64*, 557.
[22] R. L. Ball, P. Bajaj, K. A. Whitehead, *Sci. Rep.* **2018**, *8*, 2178.
[23] C. Kriegel, H. Attarwala, M. Amiji, *Adv. Drug Delivery Rev.* **2013**, *65*, 891.
[24] S. Akhtar, *J. Drug Targeting* **2009**, *17*, 491.
[25] K. A. Hajj, K. A. Whitehead, *Nat. Rev. Mater.* **2017**, *2*, 17056.
[26] A. J. Mukalel, R. S. Riley, R. Zhang, M. J. Mitchell, *Cancer Lett.* **2019**, *458*, 102.
[27] A. Schroeder, C. G. Levins, C. Cortez, R. Langer, D. G. Anderson, *J. Intern. Med.* **2010**, *267*, 9.
[28] K. Garber, *Nat. Biotechnol.* **2018**, *36*, 777.
[29] K. A. Whitehead, J. R. Dorkin, A. J. Vegas, P. H. Chang, J. Matthews, O. S. Fenton, Y. Zhang, K. T. Olejnik, V. Yesilyurt, D. Chen, S. Barros, B. Klebanov, T. Novobrantseva, R. Langer, D. G. Anderson, *Nat. Commun.* **2014**, *5*, 4277.
[30] Y. Granot, D. Peer, *Semin. Immunol.* **2017**, *34*, 68.
[31] A. K. Varkouhi, M. Scholte, G. Storm, H. J. Haisma, *J. Controlled Release* **2011**, *151*, 220.
[32] S. J. Allison, J. Milner, *Mol. Ther. – Nucleic Acids* **2014**, *3*, e141.
[33] K. J. Kauffman, J. R. Dorkin, J. H. Yang, M. W. Heartlein, F. Derosa, F. F. Mir, O. S. Fenton, D. G. Anderson, *Nano Lett.* **2015**, *15*, 7300.
[34] P. Artursson, J. Karlsson, *Biochem. Biophys. Res. Commun.* **1991**, *175*, 880.
[35] R. L. Ball, C. M. Knapp, K. A. Whitehead, *PLoS One* **2015**, *10*, e0133154.
[36] E. Blanco, H. Shen, M. Ferrari, *Nat. Biotechnol.* **2015**, *33*, 941.
[37] M. J. Mitchell, R. K. Jain, R. Langer, *Nat. Rev. Cancer* **2017**, *17*, 659.
[38] K. Paunovska, C. D. Sago, C. M. Monaco, W. H. Hudson, M. G. Castro, T. G. Rudoltz, S. Kalathoor, D. A. Vanover, P. J. Santangelo, R. Ahmed, A. V. Bryksin, J. E. Dahlman, *Nano Lett.* **2018**, *18*, 2148.

[39] Y. S. S. Yang, P. U. Atukorale, K. D. Moynihan, A. Bekdemir, K. Rakhra, L. Tang, F. Stellacci, D. J. Irvine, *Nat. Commun.* **2017**, *8*, 1.
[40] Z. Yaari, D. Da Silva, A. Zinger, E. Goldman, A. Kajal, R. Tshuva, E. Barak, N. Dahan, D. Hershkovitz, M. Goldfeder, J. S. Roitman, A. Schroeder, *Nat. Commun.* **2016**, *7*, 13325.
[41] J. E. Dahlman, K. J. Kauffman, Y. Xing, T. E. Shaw, F. F. Mir, C. C. Dlott, R. Langer, D. G. Anderson, E. T. Wang, *Proc. Natl. Acad. Sci. USA* **2017**, *114*, 2060.
[42] A. Wroblewska, M. Dhainaut, B. Ben-Zvi, S. A. Rose, E. S. Park, E.-A. D. Amir, A. Bektesevic, A. Baccarini, M. Merad, A. H. Rahman, B. D. Brown, *Cell* **2018**, *175*, 1141.
[43] P. P. G. Guimaraes, R. Zhang, R. Spektor, M. Tan, A. Chung, M. M. Billingsley, R. El-Mayta, R. S. Riley, L. Wang, J. M. Wilson, M. J. Mitchell, *J. Controlled Release* **2019**, *316*, 404.
[44] K. Paunovska, C. J. Gil, M. P. Lokugamage, C. D. Sago, M. Sato, G. N. Lando, M. G. Castro, A. V. Bryksin, J. E. Dahlman, *ACS Nano* **2018**, *12*, 8341.
[45] K. T. Love, K. P. Mahon, C. G. Levins, K. A. Whitehead, W. Querbes, J. R. Dorkin, J. Qin, W. Cantley, L. L. Qin, T. Racie, M. Frank-Kamenetsky, K. N. Yip, R. Alvarez, D. W. Y. Sah, A. De Fougerolles, K. Fitzgerald, V. Koteliansky, A. Akinc, R. Langer, D. G. Anderson, *Proc. Natl. Acad. Sci. USA* **2010**, *107*, 1864.
[46] P. R. Cullis, M. J. Hope, *Mol. Ther.* **2017**, *25*, 1467.
[47] Y. Zhao, L. Huang, *Adv. Genet.* **2014**, 13.
[48] M. Ramezanpour, M. L. Schmidt, I. Bodnariuc, J. A. Kulkarni, S. S. W. Leung, P. R. Cullis, J. L. Thewalt, D. P. Tieleman, *Nanoscale* **2019**, *11*, 14141.
[49] Y. Wang, L. Miao, A. Satterlee, L. Huang, *Adv. Drug Delivery Rev.* **2015**, *87*, 68.
[50] Q. Cheng, T. Wei, L. Farbiak, L. T. Johnson, S. A. Dilliard, D. J. Siegwart, *Nat. Nanotechnol.* **2020**, *15*, 313.
[51] I. Pereira De Sousa, C. Steiner, M. Schmutzler, M. D. Wilcox, G. J. Veldhuis, J. P. Pearson, C. W. Huck, W. Salvenmoser, A. Bernkop-Schnürch, *Eur. J. Pharm. Biopharm.* **2015**, *97*, 273.
[52] T. L. Jensen, M. K. Kiersgaard, D. B. Sørensen, L. F. Mikkelsen, *Lab. Anim.* **2013**, *47*, 225.
[53] M. Durán-Lobato, I. Muñoz-Rubio, M. Á. Holgado, J. Álvarez-Fuentes, M. Fernández-Arévalo, L. Martín-Banderas, *J. Biomed. Nanotechnol.* **2014**, *10*, 1068.
[54] M. Thanou, J. C. Verhoef, H. E. Junginger, *Adv. Drug Delivery Rev.* **2001**, *52*, 117.
[55] A. B. Bialkowska, A. M. Ghaleb, M. O. Nandan, V. W. Yang, *J. Visualized Exp.* **2016**, *2016*, 54161.
[56] M. Yoneda, A. A. Molinolo, J. M. Ward, S. Kimura, R. A. Goodlad, *J. Visualized Exp.* **2015**, *2015*, e53042.
[57] J. Xu, Y. Lin, P. Boulas, M. L. Peterson, *Expert Opin. Drug Delivery* **2018**, *15*, 197.
[58] J. Woodley, *Clin. Pharmacokinet.* **2001**, *40*, 77.
[59] A. des Rieux, V. Fievez, M. Garinot, Y. J. Schneider, V. Préat, *J. Controlled Release* **2006**, *116*, 1.
[60] S. K. Lai, Y.-Y. Wang, J. Hanes, *Drug Delivery* **2009**, *61*, 158.
[61] J. Mestecky, Z. Moldoveanu, M. Novak, W. Q. Huang, R. M. Gilley, J. K. Staas, D. Schafer, R. W. Compans, *J. Controlled Release* **1994**, *28*, 131.
[62] I. Behrens, A. I. V. Pena, M. J. Alonso, T. Kissel, *Pharm. Res.* **2002**, *19*, 1185.
[63] M. Liu, J. Zhang, W. Shan, Y. Huang, *Asian J. Pharm. Sci.* **2015**, *10*, 275.
[64] H. Yuan, C. Y. Chen, G. H. Chai, Y.-Z. Du, F. Q. Hu, *Mol. Pharmaceutics* **2013**, *10*, 1865.
[65] Q. Xu, L. M. Ensign, N. J. Boylan, A. Schön, X. Gong, J. C. Yang, N. W. Lamb, S. Cai, T. Yu, E. Freire, J. Hanes, *ACS Nano* **2015**, *9*, 9217.
[66] K. Maisel, M. Reddy, Q. Xu, S. Chattopadhyay, R. Cone, L. M. Ensign, J. Hanes, *Nanomedicine* **2016**, *11*, 1337.
[67] A. A. Date, J. Hanes, L. M. Ensign, *J. Controlled Release* **2017**, *176*, 139.
[68] Y. Yamanashi, T. Takada, R. Kurauchi, Y. Tanaka, T. Komine, H. Suzuki, *J. Atheroscler. Thromb.* **2017**, *24*, 347.
[69] P. W. Laird, A. Zijderveld, K. Linders, M. A. Rudnicki, R. Jaenisch, A. Berns, *Nucleic Acids Res.* **1991**, *19*, 4293.

